ISSN 2072-5981
doi: 10.26907/mrsej

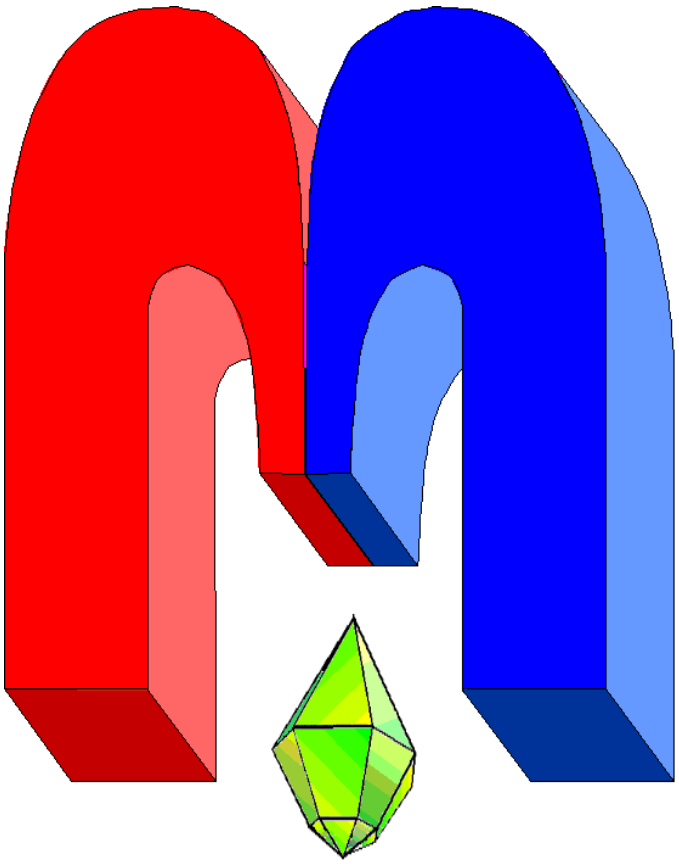

# Magnetic Resonance in Solids

Electronic Journal

*Volume* ***26***
*Issue* ***1***
*Article No* ***24103***
*1-11 pages*
*April,* ***19***
***2024***
doi: **10.26907/mrsej-24103**

**http://mrsej.kpfu.ru**
**https://mrsej.elpub.ru**

Established and published by Kazan University*
Endorsed by International Society of Magnetic Resonance (ISMAR)
Registered by Russian Federation Committee on Press (#015140), August 2, 1996
First Issue appeared on July 25, 1997



"***Magnetic Resonance in Solids. Electronic Journal***" (**MRS*ej***) is a peer-reviewed, all electronic journal, publishing articles which meet the highest standards of scientific quality in the field of basic research of a magnetic resonance in solids and related phenomena.

Indexed and abstracted by
*Web of Science* (*ESCI*, Clarivate Analytics, from 2015), *Scopus* (Elsevier, from 2012), *RusIndexSC* (*eLibrary*, from 2006), *Google Scholar*, *DOAJ*, *ROAD*, *CyberLeninka* (from 2006), *SCImago Journal & Country Rank*, etc.



* Address: "Magnetic Resonance in Solids. Electronic Journal", Kazan Federal University; Kremlevskaya str., 18; Kazan 420008, Russia

† In Kazan University the Electron Paramagnetic Resonance (EPR) was discovered by Zavoisky E.K. in 1944.

Short cite this: *Magn. Reson. Solids* **26**, 24103 (2024) doi: 10.26907/mrsej-24103

# Synthesis and study of the cerium doped hydroxyapatite powders†

Y.O. Nikitina[1], N.V. Petrakova[1], E.I. Maksimenko[1], S.V. Chizhevskaya[2], S.M. Andreev[3], M.A. Sadovnikova[4], F.F. Murzakhanov[4*], G.V. Mamin[4], M.R. Gafurov[4], V.S. Komlev[1]

[1] A.A. Baikov Institute of Metallurgy and Materials Science RAS, Moscow 119334, Russia
[2] D. Mendeleyev University of Chemical Technology of Russia, Moscow 125480, Russia
[3] St.Petersburg State University, Peterhof 198504, Russia
[4] Kazan Federal University, Kazan 420008, Russia

**E-mail: murzakhanov.fadis@yandex.ru*

(Received November 20, 2023; accepted April 15, 2024; published April 19, 2024)

Hydroxyapatite (HAp) is an attractive material for creating biocompatible implants owing to its osteoregenerative properties, elemental and phase similarity to bone tissue. The flexible structure of the material allows the introduction of ionic impurities to improve physicochemical and biological characteristics while maintaining the space symmetry group. Rare earth ions are a new step in improving compounds to create luminescent bioimaging agent for application in diagnostics imaging medicine. Nanosized powder of HAp doped with cerium ions (Ce-HAp) was obtained in order to study the impurity localization and its oxidizing state with conventional and pulsed electron paramagnetic resonance (EPR) at X-band. Undoped and doped HAp powders were synthesized via precipitation technique. It was revealed, that Ce-HAp powders after synthesis and heating exhibit luminescence in visible wavelength range (380 and 420 nm) that confirms the presence of $Ce^{3+}$ in HAp structure. Heating of Ce-HAp in the air atmosphere results in formation of $CeO_2$ with low intensity of luminescence. EPR spectra of the doped sample confirms the $Ce^{3+}$ incorporation into HAp structure. The powder-like EPR lineshape for the obtained powders can be simulated with $g_{\parallel} = 3.47$ and $g_{\perp} = 0.51$.

**PACS:** 76.30.-v, 76.30.Kg, 76.60.Lz, 78.55.-m

**Keywords:** electron paramagnetic resonance, electron spin echo, hydroxyapatite, rare earth element, photoluminescence

## 1. Introduction

Search for materials for the restoration of osteochondral defects resulting from injury and disease remains one of the main challenges in the field of materials science and tissue engineering. One of the most used bioactive synthetic materials for bone replacement is calcium hydroxyapatite (HAp), which is the main mineral component of bone tissue, tooth enamel and dentin. HAp exhibits the greatest resistance to resorption by biological fluids of the body among calcium phosphates [1–3]. HAp-based compounds possess high isomorphic capacity with respect to cations and anions [4, 5]. Currently, natural and synthetic apatites are used not only for the biomedical applications, but also as raw materials for the production of mineral fertilisers, pure phosphorus and phosphoric acid, for lasers, immobilisation of radioactive waste, as ionic conductors, sorbents, inorganic pigments [6].

In a series of our papers, we published the results of our comprehensive research concerning synthesis, structural, physical, chemical, and biological properties for the HAp-substituted bulk and nanosized powders, ceramics, cements, coatings, and composites [7–13]. Since recently, calcium phosphates doped with the rare-earth elements (REEs) have attracted our attention [12,13]. We have also demonstrated in the mentioned above papers that various electron paramagnetic resonance (EPR) techniques can be fruitfully used for the structural characterization of the

†This paper is dedicated to Professor Boris I. Kochelaev on the occasion of his 90th birthday.

substituted HAp. Some studies of various apatites with rare earth dopants show their site preference for the Ca(2) position in the atomic arrangement of calcium phosphates [14]. The ratios of REE-Ca(2)/REE-Ca(1) vary between 1.76 and 3.00, decreasing monotonically with atomic number through the 4f transition series. Different radii constraints, bonds valence, mean tetrahedral bond distances and multiplicity of coordination number requirements influence on the substitution of calcium by REEs. Lighter REEs tend to prefer the Ca(2) site, while heavier REEs may occupy both Ca sites. Bond valence analysis suggests that Gd, La, Ce, and Pr incorporate into the Ca(2) site, while Pm and Sm prefer the Ca(1) position, and Nd ions show a preference for both sites [14, 15].

The introduction of $Ce^{3+}$ ions into the structure of HAp makes it possible to obtain a material that has antibacterial properties to counteract inflammation in the postoperative period, antitumor properties, etc. [16–19]. In addition, the ability of cerium to luminesce allows the use of HAp doped with cerium ions as a biomarker of biological visualization for monitoring processes involved in the reconstruction of bone defects [20–22]. However, the synthesis of Ce-HAp is associated with several problems, the main of which is the instability of the valence state (transition of $Ce^{3+}$ to $Ce^{4+}$ in air [23]) with the loss of the beneficial properties described above. In addition, the substitution of the $Ca^{2+}$ ion by the $Ce^{3+}$ ion is complicated due to the difference in their charges [24–27]. To prevent the transition of $Ce^{3+}$ to $Ce^{4+}$ in air when producing ceramics based on hydroxyapatite, it was proposed to apply a powder consolidation method such as hot pressing under an inert environment, for example, argon [28]. The purpose of this work was to synthesize and study hydroxyapatite doped with cerium(III) to obtain functional ceramics and to study the capabilities of the EPR methods for studying the obtained samples.

## 2. Synthesis

Undoped hydroxyapatites and Ce-containing hydroxyapatites (Ce-HAp) were synthesized via precipitation technique with accordance to the reaction (1) in the way to keep the total molar ratio $(M_{Ca} + M_{Ce})/M_P = 1.67$.

$$\begin{aligned}(10-x)Ca(NO_3)_2 + (2x/3)Ce(NO_3)_3 + 6(NH_4)_2HPO_4 + 8NH_4OH \rightarrow \\ \rightarrow Ca_{10-x}Ce_{2x/3}(PO_4)_6(OH)_2 + 6H_2O + 20NH_4NO_3,\end{aligned} \quad (1)$$

where $x$ is a degree of substitution, $x = ([Ca^{2+}] \times [Ce^{3+}])/100$; $[Ca^{2+}]$ is an atomic content of $Ca^{2+}$ in HAp, $[Ce^{3+}]$ is an atomic content of $Ce^{3+}$ in Ce-HAp; $[Ce^{3+}] = 0$ and 0.5 for $[Ca^{2+}]$.

The amount of Ce ([Ce]) was calculated of 0.5 in respect to Ca atomic content in HAp ([Ca]): thus, for HAp [Ca]=10, the amount of Ce was taken of 0.5 for [Ca], therefore [Ce] = $(10 \times 0.5)/100$. For this, the 0.5 M aqueous solution of ammonium hydrophosphate ($(NH_4)_2HPO_4$) was dropwise added to the mix of 0.5 M solution of calcium nitrate ($Ca(NO_3)_2$) and 0.1 M solution of cerium nitrate ($Ce(NO_3)_2$) in appropriate amount under constant stirring. The pH level was adjusted at $11.0 \pm 0.5$ by adding the ammonium hydroxide solution ($NH_4OH$). The resulted suspensions were kept for aging for 24 h under room conditions, then were filtered and dried at 70°C during 48 h. The dried cakes were ground to a fine powder and sieved through a mesh size of 100 $\mu$m.

As-dried powders were heat treated under different conditions: (i) the heat treating at 1300° C in air atmosphere (Ce-HAp-air) in a chamber furnace with SiC heaters and (ii) hot pressing (Ce-HAp-HP) in a hot press furnace (Thermal technology Inc., model HP 250-3560-20) in a carbon mold in an argon atmosphere at a pressure of 30 MPa and temperature of 1100° C to achieve the reducing atmosphere.

The obtained Ce-HAp materials were studied on phase composition and Ce content by the following methods: EPR spectroscopy, X-ray diffraction (XRD) analysis, determination of the specific surface area (SSA) and X-ray fluorescence spectrometry (XFS).

## 3. Methods

The magnetic resonance experiments were carried out with a Bruker Elexsys E580 commercial spectrometer operated at 9.6 GHz (X-band) in the continuous wave (CW) and pulsed modes. The EPR spectra were recorded by detecting the amplitude of the primary electron spin echo (ESE) as a function of the magnetic field sweep using a pulse sequence $\pi/2 - \tau - \pi - \tau -$ ESE, where $\pi/2 = 12$ ns and $\tau = 200$ ns.

The XRD patterns were collected on XRD-6000 powder diffractometer (Bragg-Brentano geometry, Scintillator detector, CuK$\alpha$ radiation, $\lambda = 1.5418$ Å, Shimadzu, Japan). The XRD data were recorded at room temperature in the $2\theta$ range between 10° and 60°, with intervals of 0.02°, and a counter speed of 2°/min. The element content of cerium [Ce] for the Ce-HAp powders was determined using the XFS Spectroscan MAKC-GVM spectrometer (St. Petersburg, Russia).

Specific surface area of the powders was measured using the Brunauer-Emmett-Teller (BET) method of low-temperature nitrogen adsorption on a Tristar 3000 analyser (Micromeritics, USA). The particle average diameter ($D_{\mathrm{BET}}$) was calculated according to formula (2):

$$D_{\mathrm{BET}} = \frac{6000}{\mathrm{SSA} \cdot \rho}, \tag{2}$$

where $\rho$ is theoretical density for HAp ($3.156\ \mathrm{g \cdot cm^{-3}}$).

Photoluminescence emission spectra were recorded on LS-55 spectrometer (Perkin Elmer Inc., USA) with a xenon light source (power 150 W, pulse frequency 50 Hz, wavelength resolution 0.5 nm, $\lambda_{\mathrm{exc}} = 270$ nm, $\lambda_{\mathrm{em}} = 300 \div 500$ nm) at room temperature.

## 4. Results

The elemental analysis using XFS spectroscopy was performed on the Ce-HAp powder preheated at 1300°C in order to remove the inorganic salts and crystallohydrate water accompanying to the precipitation. The Ce content in Ce-HAp was measured to be 2.21 wt.%, that was higher than expected (1.18 wt.%) and could be recalculated as 0.78 mol.% Ce in the compound. SSA of the as-dried powder was $130\ \mathrm{m^2 \cdot g^{-1}}$ that in recalculation on the average particle size ($D_{\mathrm{BET}}$) was 15 nm.

XRD patterns of as-dried powders indicated the presence of an amorphous state of HAp (JCPDS card [09-0342]) (Figure 1). The set of low-intensity broadened XRD peaks was assigned to the set of HAp peaks. However, in XRD of Ce-HAp the peak at $2\theta = 29.3°$ was assigned to cerium phosphate $CePO_4$ (JCPDS card [04-0632]) that was absent on the pattern for undoped HAp. The XRD for Ce-HAp-air and Ce-HAp-HP concided with the well-crystallized HAp (card [09-0432]). The patten for Ce-HAp contained a weak peak at $2\theta = 28.5°$, assigned to cerium oxide, $CeO_2$ (card [81-0792]). Thus, it was concluded that during the precipitation under high pH level, the mix of calcium HAp and cerium phosphate was formed. According to ref. [29], the low-temperature cerium orthophosphate crystallizes in hexagonal structure that is isostructural to HAp and facilitates the isomorphic substitution in its crystal lattice. Then, during the following heat treating in reducing atmosphere by hot pressing method, the $CePO_4$ redistributes in the HAp lattice as a result of high temperature diffusion to form solid solutions in a low range of dopant concentration (up to 1 at.%). When Ce-HAp is heat treated in the air atmosphere, the

Ce oxidation state changes with the $CeO_2$ formation [28].

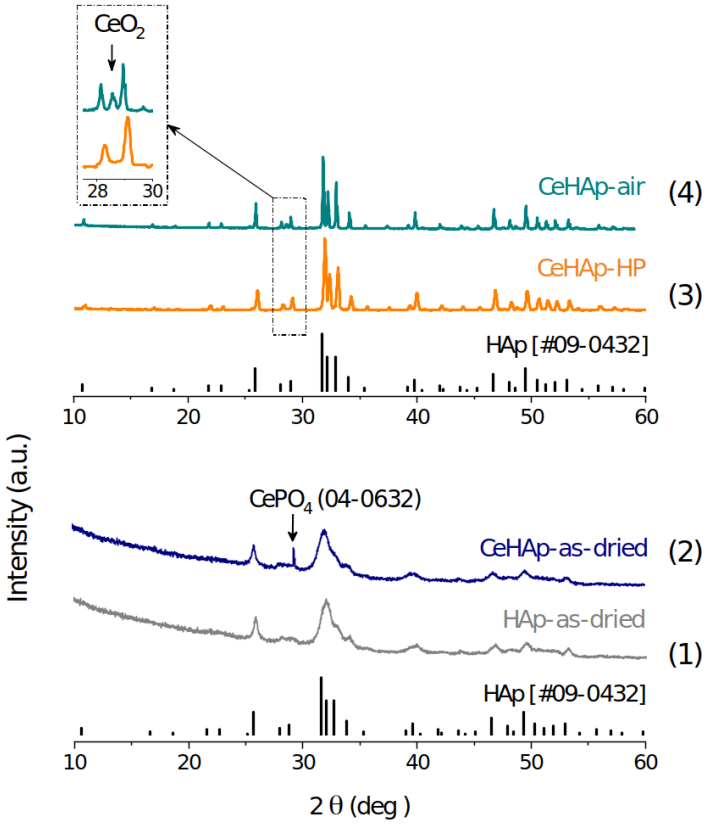


**Figure 1.** XRD patterns for undoped HAp and Ce-HAp: (1) – pattern for undoped as-dried HAp quite consistent with the HAp card [09-0432], (2) – pattern for as-dried Ce-HAp indicates the presence of $CePO_4$ [04-0632], (3) – pattern for Ce-HAp obtained by hot pressing in reducing atmosphere fully correspond to HAp card without any impurity; (4) – pattern for Ce-HAp obtained by heat treating in air atmosphere contains the $CeO_2$ impurity.

The influence of Ce content was estimated in respect to the changes of average crystallinity size and parameters of HAp crystal lattice (Table 1). The average crystallinity size ($D$) of as-dried powders was $14 \div 16$ nm that was equal to SSA estimation. It was revealed that as a result of heat treating in air, the lattice parameters for Ce-HAp became practically the same as for the undoped HAp. During hot pressing the simultaneous sintering and densification occurred that resulted in crystal lattice improvements and in slight decreasing of lattice parameters [30, 31].

**Table 1.** The effect of the treating conditions on the average crystallinity size $D$ and lattice parameters ($a$ and $c$) of HAp.

| Sample | $D$ (±10%), nm | $a$ parameter (±0.002), Å | $c$ parameter (±0.002), Å |
|---|---|---|---|
| as-dried HAp | 16 | — | — |
| as-dried Ce-HAp | 14 | — | — |
| HAp-air | 90 | 9.422 | 6.883 |
| Ce-HAp-air | 80 | 9.421 | 6.883 |
| HAp-HP | 75 | 9.402 | 6.872 |
| Ce-HAp-HP | 60 | 9.398 | 6.869 |

Figure 2 demonstrates that as-dried Ce-HAp powder exhibits luminescence in visible wavelength range. The luminescence of Ce-HAp consists of emission of the $Ce^{3+}$ ion (380 and 420 nm) [32, 33] and the intrinsic emission of HAp (406 and 420 nm) [34, 35]. Ce-HAp-air exhibits the lowest luminescence emission due to presence of $CeO_2$. The Ce-HAp-HP shows the highest luminescence intensity.

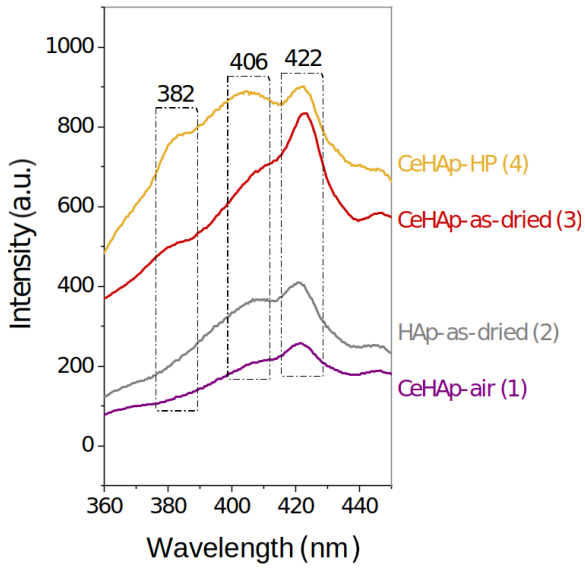


**Figure 2.** Photoluminescence spectra for Ce-HAp obtained by different methods: Ce-HAp heat treated in air (1), as-dried powders of HAp (2), Ce-HAp (3), and hot pressed Ce-HAp (4).

In CW EPR spectrum of the Ce-HAp-as-dried sample (Figure 3A) one can observe lines at $g$-factors of 4.2, 3.47, a group of lines around of $g = 1.98$, and a wide peak at $g = 0.51$. The EPR spectrum in pulsed mode is shown in the (Figure 3B). The attenuation of the microwave power of pulses in Hahn sequence (high power attenuation, HPA) was varied from 0 to 12 dB. As can be seen from Figure 3B, in the magnetic field range from 0.2 T to 1.4 T (maximal magnetic field value for the spectrometer), a broad line is observed. Due to its high intensity and absence of such kind of signal in the non-doped samples we can attribute it to the presence of the paramagnetic $Ce^{3+}$ ions.

The line at $g$-factor 4.2 from CW EPR disappears in the pulsed regime, and can be ascribed to uncontrolled impurities of the iron group complexes [7] with concentration $< 0.001$ mol.% in HAp. The group of lines at $g = 1.98$ behaves differently with a change in microwave power than the broad one. A weakly expressed hyperfine structure of 6 lines is also observed, which allows us to attribute this group of lines to the $Mn^{2+}$ ions (an uncontrolled impurity with concentration $< 0.01$ mol.%) [36].

In a rotating coordinate system, the Rabi frequency for the precession $\omega_1$ around the magnetic component $B_1$ of the microwave field can be described by the following expression [37]:

$$\omega_1 = \frac{g\mu_B}{\hbar} B_1 \sqrt{S(S+1) - M_S(M_S+1)}, \tag{3}$$

where $B_1$ is an amplitude of the magnetic component of the microwave irradiation, $\mu_B$ is a Bohr magneton, $g$ is a $g$-factor, $S$ is an electron spin and $M_S$ is a spin projection quantum number.

It gave us an opportunity to estimate the value of $B_1 = 0.33$ mT for HPA $= 4$ dB from measuring $\omega_1$ for $Mn^{2+}$ for the central EPR transition ($S = 5/2$, $M_S = -1/2$). Details of measuring $\omega_1$ are given below.

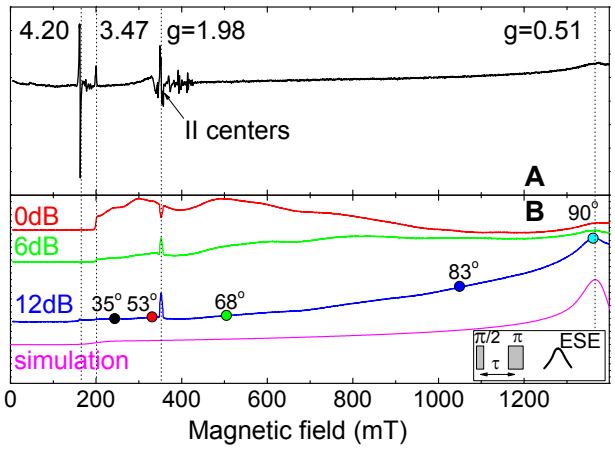


**Figure 3.** EPR spectrum of $Ce^{3+}$ ions in Ce-HAp. A – spectrum recorded in CW mode. B – spectrum recorded in pulse mode at different microwave pulse powers (HPA of 0, 6 and 12 dB). The dots on the Figure 3B show the values of the magnetic fields in which Rabi oscillations were measured; the number correspond to the value of $\theta$ angle particles relative to $B_0$. Magenta curve – EPR spectrum simulated in Easyspin program [38] for $g_{\|} = 3.47$ and $g_{\perp} = 0.51$

The broad EPR line of $Ce^{3+}$ ions has a shape that is not characteristic for the powder. Additonally, the lineshape changes greatly with microwave power (Figure 3B). For single crystals, these are the signs for detection of various electron transitions with different values of the operator $\langle M_1|S_x|M_2\rangle$. To check this effect, Rabi oscillations at various spectral positions were measured from the dependence of the ESE amplitude $A_{\mathrm{ESE}}$ (Figure 4) by using the three-pulse sequence (preparation pulse with the varied duration from 4 to 4100 ns ($\tau_{\mathrm{first\ pulse}}$) followed by the Hahn pulse sequence after 15 $\mu$s).

$$A_{\mathrm{ESE}} = \sin\left(\omega_1 \tau_{\mathrm{first\ pulse}}\right) \exp\left(\frac{\tau_{\mathrm{first\ pulse}}}{T_2}\right). \tag{4}$$

The experimental data in Figure 4 show smooth change of the oscillation period with increasing magnetic field and a fairly rapid decrease in the oscillation amplitude compared to the transverse relaxation time $T_2 = 2.9 \pm 0.5\,\mu$s.

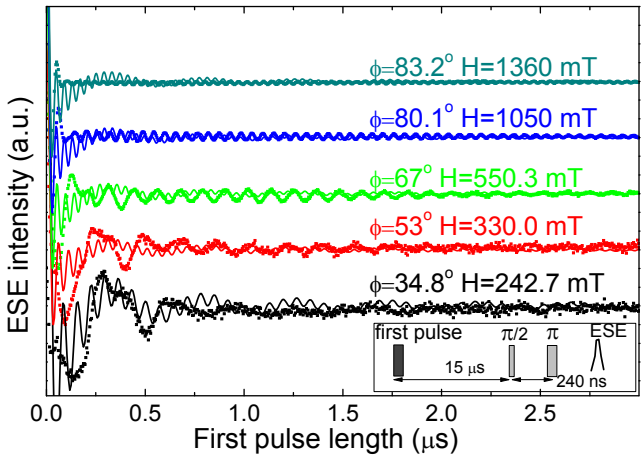


**Figure 4.** Rabi oscillations measured at the same microwave power (HPA = 4 dB) for different values of the magnetic field. Dots show experimental data, lines show calculation data using Eq. (13)

The $Ce^{3+}$ ion has only one 4f electron, the $^4f_1$ ground state configuration of which gives two multiplets: the lower $^2F_{5/2}$ and the upper $^2F_{7/2}$ [39]. In YAG crystals, the lower doublet of $Ce^{3+}$ ions is characterized by $g$-factors from 2.5 to 0.9 [40]. Cerium has only even isotopes with zero nuclear magnetic moment ($I = 0$), so the hyperfine structure of the EPR spectra is not observed.

Crystallites of HAp powder, according to XRD analysis, have a hexagonal crystal structure ($P6_3/m$). For Ca ions, there are two nonequivalent positions: Ca(1) with the $C_3$ point group, and Ca(2) with the lower symmetry $C_{1h}$. For Ca(1), the EPR spectrum should be described by the Hamiltonian of axial symmetry

$$\hat{\mathcal{H}} = \begin{pmatrix} 0 & 0 & B_0 \end{pmatrix} \begin{bmatrix} g_\perp & 0 & 0 \\ 0 & g_\perp & 0 \\ 0 & 0 & g_\parallel \end{bmatrix} \begin{pmatrix} S_x \\ S_y \\ S_z \end{pmatrix}, \tag{5}$$

where the main **z** axis of the $g$-tensor is directed along the **c** axis of the crystallite, and **x** and **y** are located in the **ab** plane. If the Ca(2) position is replaced, the $g$-tensor will contain three different components $g_{xx}$, $g_{yy}$, $g_{zz}$, and the main axes of the tensor will be deviated from the crystal axes directions.

$$\hat{\mathcal{H}} = \begin{pmatrix} 0 & 0 & B_0 \end{pmatrix} \begin{bmatrix} g_{xx} & 0 & 0 \\ 0 & g_{yy} & 0 \\ 0 & 0 & g_{zz} \end{bmatrix} \begin{pmatrix} S_x \\ S_y \\ S_z \end{pmatrix}, \tag{6}$$

Note that for the case of low symmetry, the main directions of the $g$-tensor can differ from the directions of the crystal axes. But since the directions of the crystalline axes for particles in the powder are distributed uniformly over the solid angle, then the main directions of the $g$-tensor will also be distributed uniformly. Therefore, the direction cosines of the $g$-tensor do not manifest themselves in any way in the case of powder-like spectral patterns, and cannot be determined by powder EPR spectroscopy.

Let us consider the behavior of $\omega_1$ for such wide lines. The rotation of the spherical coordinate system for individual particles is carried out by multiplying the rotation matrix

$$\begin{bmatrix} \cos\phi\cos\theta & -\sin\phi & -\sin\theta\cos\phi \\ \sin\phi\cos\theta & \cos\phi & -\sin\phi\sin\theta \\ \sin\theta & 0 & \cos\theta \end{bmatrix}, \tag{7}$$

by the $g$-tensor.

It allows calculating the $g$-factor for each of the particles in axial symmetry case

$$g_{\text{eff}}(\theta)(\text{I}) = \sqrt{g_\parallel^2 \cos^2\theta + g_\perp^2 \sin^2\theta} \tag{8}$$

and for the low symmetry case

$$g_{\text{eff}}(\theta)(\text{II}) = \sqrt{g_{xx}^2 \sin^2\theta\cos^2\phi + g_{yy}^2 \sin^2\phi\sin^2\theta - g_{zz}^2 \cos^2\theta}. \tag{9}$$

As can be seen from Eq. (8), for axial symmetry $g_{\text{eff}}$ does not depend on the angle $\phi$. To find the frequency $\omega_1$, in the case of the direction of $B_1$ along the **x** axis, it is necessary to replace the vector $(0, 0, B_0)$ with $(B_1, 0, 0)$ in expression (5, 6).

$$g_{B_1}(\theta,\phi)(\text{I}) = \sqrt{g_\parallel^2 \sin^2\theta\cos^2\phi + g_\perp^2 \sin^2\phi + g_\perp^2 \cos^2\phi\cos^2\theta}, \tag{10}$$

$$g_{B_1}(\theta,\phi)(\mathrm{II}) = \sqrt{g_{xx}^2\cos^2\phi\cos^2\theta + g_{yy}^2\sin^2\phi\cos^2\theta - g_{zz}^2\sin^2\theta}. \quad (11)$$

Leaving outside the brackets of this investigation the question of the location of $Ce^{3+}$ ions and to simplify calculations, the axial symmetry tensor will be further used for the spin system with the electron spin $S = 1/2$ (Figure 3B, magenta curve). For axial position the equation 10 can be simplified to

$$g_{B_1}(\theta,\phi) = \sqrt{g_{\mathrm{eff}}^2(\mathrm{I})(90^\circ-\theta)\cos^2\phi + g_\perp^2\sin^2\phi}. \quad (12)$$

Note, that even for the axial symmetry $g_{B1}$ is $\phi$-dependent. The relation between the angle $\theta$ and the value of the magnetic field induction $B_0$ is given by the expression 8. Since crystallites in powder are oriented randomly relative to the angles $\theta$ and $\phi$, ESE amplitude without taking $T_2$ into account will be described by the formula:

$$A_{\mathrm{ESE}} = \frac{2}{\pi}\int_0^{\pi/2}\sin\left(\frac{g_{B_1}(\theta,\phi)(\mathrm{I})\mu_{\mathrm{B}}}{\hbar}B_1\tau_{\text{first pulse}}\right)d\phi, \quad (13)$$

In the case of low symmetry, such a simple formula cannot be obtained, since for a given orientation of magnetic field, a set of powder particles with different $\phi$ and $\theta$. Therefore, it is impossible to obtain an expression for the amplitude $A_{\mathrm{ESE}}$.

Calculations performed using expressions (12), (13) are shown in Figure 4 by solid lines. As can be seen from the Figure 4, averaging harmonic signals with different frequencies leads to rapid attenuation of Rabi oscillations, but two components corresponding to the limits:

$$\omega_{1,\mathrm{low}} = \frac{g_{\mathrm{eff}}^2(90^\circ-\theta)\mu_{\mathrm{B}}}{\hbar}B_1 \quad (14)$$

and

$$\omega_{1,\mathrm{high}} = \frac{g_\perp\mu_{\mathrm{B}}}{\hbar}B_1, \quad (15)$$

remain pronounced.

It should be noted that the presented calculations do not take into account additional mechanisms of averaging by the distribution of $g_\perp$ (in Figure 3B, the high-field part of the spectrum has a larger width than the low-field one), which, in accordance with (12) will lead to additional averaging of Rabi oscillations and suppression of the high-frequency component.

## 5. Conclusions

In this article a hydroxyapatite powders with the impurity rare earth cerium ions were synthesized and analyzed by X-ray, photoluminescence and EPR spectroscopy. XRD shows that the temperature treatment of the samples leads to a significant increase in the crystallinity degree of a hydroxyapatite. Intense luminescence spectra of $Ce^{3+}$ ions in the visible range (380 nm and 420 nm) promise of using cerium-doped hydroxyapatite as a contrast agent for biomedical applications. EPR studies confirmed the presence of $Ce^{3+}$ in the HAp structure. Application of the pulsed EPR techniques made it possible to determine the values of the components of $g$-factor. It was observed that EPR lineshape is distorted compared to the classical powder-like EPR spectrum due to the large anisotropy of $g$-factor components. To correctly record such EPR spectra using pulsed EPR techniques methods, it can be recommended to acquire the EPR spectra at the microwave power value which is lower than the optimal one. Regrettably, based on the results presented in this paper, the authors have refrained from delving into the precise localization of cerium ions due to the broad EPR spectrum, including a structureless

line that hinders detailed analysis. Further investigations utilizing electron-nuclear double resonance techniques are planned to be applied for detecting signals from neighboring nuclei such as hydrogen $^{1}$H and phosphorus $^{31}$P, with aim to estimate the interatomic distances for RE dopants.

## Acknowledgments

Authors acknowledge the Russian Science Foundation Grant No. 23-23-00640 for financial support of this study.

## References

1. Roberts T. T., Rosenbaum A. J., *Organogenesis* **8**, 114 (2012).

2. Le Huec J., Schaeverbeke T., Clement D., Faber J., Le Rebeller A., *Biomaterials* **16**, 113 (1995).

3. Hench L. L., *Journal of the American Ceramic Society* **74**, 1487 (1991).

4. Tite T., Popa A., Balescu L., Bogdan I., Pasuk I., Ferreira J., Stan G., *Materials (Basel)* **11**, 1 (2018).

5. Boanini E., Gazzano M., Bigi A., *Acta Biomaterialia* **6**, 1882 (2010).

6. Guesmi Y., Lafi R., Agougui H., Jabli M., Oun A., Majumdar S., Hafiane A., *Materials Chemistry and Physics* **239**, 122067 (2020).

7. Gabbasov B., Gafurov M., Starshova A., Shurtakova D., Murzakhanov F., Mamin G., Orlinskii S., *Journal of Magnetism and Magnetic Materials* **470**, 109 (2019).

8. Rau J. V., Fadeeva I. V., Fomin A. S., Barbaro K., Galvano E., Ryzhov A. P., Murzakhanov F., Gafurov M., Orlinskii S., Antoniac I., Uskoković V., *ACS Biomaterials Science and Engineering* **5**, 6632 (2019).

9. Fadeeva I. V., Lazoryak B. I., Davidova G. A., Murzakhanov F. F., Gabbasov B. F., Petrakova N. V., Fosca M., Barinov S. M., Vadala G., Uskoković V., Zheng Y., Rau J. V., *Materials Science and Engineering C* **129**, 112410 (2021).

10. Makshakova O. N., Shurtakova D. V., Vakhin A. V., Grishin P. O., Gafurov M. R., *Crystals* **11**, 1219 (2021).

11. Goldberg M., Gafurov M., Makshakova O., Smirnov V., Komlev V., Barinov S., Kudryavtsev E., Sergeeva N., Achmedova S., Mamin G., Murzakhanov F. F., Orlinskii S., *The Journal of Physical Chemistry B* **123**, 9143 (2019).

12. Sadovnikova M. A., Murzakhanov F. F., Fadeeva I. V., Forysenkova A. A., Deyneko D. V., Mamin G. V., Gafurov M. R., *Ceramics* **5**, 1154 (2022).

13. Fadeeva I. V., Deyneko D. V., Barbaro K., Davydova G. A., Sadovnikova M. A., Murzakhanov F. F., Fomin A. S., Yankova V. G., Antoniac I. V., Barinov S. M., Lazoryak B. I., Rau J. V., *Nanomaterials* **12**, 852 (2022).

14. Hughes J. M., Cameron M., Mariano A. N., *American Mineralogist* **76**, 1165 (1991).

15. Chen N., Pan Y., Weil J. A., *American Mineralogist* **87**, 37 (2002).

16. Kuang Y., He X., Zhang Z., Li Y., Zhang H., Ma Y., Wu Z., Chai Z., *Journal of Nanoscience and Nanotechnology* **11**, 4103 (2011).

17. Zheng K., Torre E., Bari A., Taccardi N., Cassinelli C., Morra M., Fiorilli S., Vitale-Brovarone C., Iviglia G., Boccaccini A. R., *Materials Today Bio* **5**, 100041 (2020).

18. Nicolini V., Malavasi G., Menabue L., Lusvardi G., Benedetti F., Valeri S., Luches P., *Journal of Materials Science* **52**, 8845 (2017).

19. Feng Z., Liao Y., Ye M., *Journal of Materials Science: Materials in Medicine* **16**, 417 (2005).

20. Kaygusuz H., Torlak E., Akın-Evingür G., Özen İ., Von Klitzing R., Erim F. B., *International Journal of Biological Macromolecules* **105**, 1161 (2017).

21. Alpaslan E., Yazici H., Golshan N. H., Ziemer K. S., Webster T. J., *ACS Biomaterials Science and Engineering* **1**, 1096 (2015).

22. Chen F., Huang P., Zhu Y.-J., Wu J., Cui D.-X., *Biomaterials* **33**, 6447 (2012).

23. Ciobanu G., Bargan A. M., Luca C., *Ceramics International* **41**, 12192 (2015).

24. Fleet M. E., Liu X., Pan Y., *Journal of Solid State Chemistry* **149**, 391 (2000).

25. Cawthray J. F., Creagh A. L., Haynes C. A., Orvig C., *Inorganic Chemistry* **54**, 1440 (2015).

26. Kazin P. E., Gazizova O. R., Karpov A. S., Jansen M., Tretyakov Y. D., *Solid State Sciences* **9**, 82 (2007).

27. Kazin P. E., Zykin M. A., Gazizova O. R., Tretyakov Y. D., *Zeitschrift für Anorganische und Allgemeine Chemie* **629**, 344 (2009).

28. Nikitina Y. O., Petrakova N., Demina A. Y., Kozyukhin S., Lysenkov A., Barinov S., Komlev V., *Russian Journal of Inorganic Chemistry* **66**, 1067 (2021).

29. Bondar I. A., Vinogradova N. V., Demyanets L. N., Ezhova Z. A., Ilyukhin V. V., Kara-Ushanov V. Y., Komissarova L. N., Lazarevski E. V., Litvin B. N., Melnikov P. P., Murashov D. A., Orlovskii V. P., Palkina K. K., Petrova M. A., Rozanov I. A., Chudinova N. N., Fotiev A. A., *Rare-Earth Compounds: Silicates, Germanates, Phosphates, Arsenates, and Vanadates* (Nauka, 1983) p. 284.

30. Veljović D., Jokić B., Petrović R., Palcevskis E., Dindune A., Mihailescu I. N., Janaćković D., *Ceramics International* **35**, 1407 (2009).

31. Petrakova N., Lysenkov A., Ashmarin A., Egorov A., Fedotov A. Y., Shvorneva L., Komlev V., Barinov S., *Inorganic Materials: Applied Research* **4**, 362 (2013).

32. Masalov A., Viagin O., Maksimchuk P., Seminko V., Bespalova I., Aslanov A., Malyukin Y., Zorenko Y., *Journal of Luminescence* **145**, 61 (2014).

33. Lin J., Yao G., Dong Y., Park B., Su M., *Journal of Alloys and Compounds* **225**, 124 (1995).

34. Gaft M., Reisfeld R., Panczer G., *Modern luminescence spectroscopy of minerals and materials* (Springer, 2015) p. 356.

35. Machado T. R., Sczancoski J. C., Beltrán-Mir H., Li M. S., Andres J., Cordoncillo E., Leite E., Longo E., *Ceramics International* **44**, 236 (2018).

36. Shurtakova D. V., Grishin P. O., Gafurov M. R., Mamin G. V., *Crystals* **11**, 1050 (2021).

37. Hofbauer W., Bittl R., *Journal of Magnetic Resonance* **147**, 226 (2000).

38. Stoll S., Schweiger A., *Journal of Magnetic Resonance* **178**, 42 (2006).

39. Edinach E., Uspenskaya Y. A., Gurin A. S., Babunts R. A., Asatryan G. R., Romanov N. G., Badalyan A. G., Baranov P. G., *Physics of the Solid State* **61**, 1820 (2019).

40. Asatryan G., Kramushchenko D., Uspenskaya Y. A., Baranov P., Petrosyan A., *Physics of the Solid State* **56**, 1150 (2014).